JACS
JOURNAL OF THE AMERICAN CHEMICAL SOCIETY

Article

pubs.acs.org/JACS

Electron Transfer within Self-Assembling Cyclic Tetramers Using Chlorophyll-Based Donor–Acceptor Building Blocks

Victoria L. Gunderson, Amanda L. Smeigh, Chul Hoon Kim, Dick T. Co, and Michael R. Wasielewski*

Department of Chemistry and Argonne-Northwestern Solar Energy Research (ANSER) Center, Northwestern University, Evanston Illinois 60208-3113, United States

Supporting Information

ABSTRACT: The synthesis and photoinduced charge transfer properties of a series of Chl-based donor–acceptor triad building blocks that self-assemble into cyclic tetramers are reported. Chlorophyll *a* was converted into zinc methyl 3-ethylpyrochlorophyllide *a* (Chl) and then further modified at its 20-position to covalently attach a pyromellitimide (PI) acceptor bearing a pyridine ligand and one or two naphthalene-1,8:4,5-bis(dicarboximide) (NDI) secondary electron acceptors to give Chl–PI–NDI and Chl–PI–NDI_2. The pyridine ligand within each ambident triad enables intermolecular Chl metal–ligand coordination in dry toluene, which results in the formation of cyclic tetramers in solution, as determined using small- and wide-angle X-ray scattering at a synchrotron source. Femtosecond and nanosecond transient absorption spectroscopy of the monomers in toluene–1% pyridine and the cyclic tetramers in toluene shows that the selective photoexcitation of Chl results in intramolecular electron transfer from ^{1}*Chl to PI to form $Chl^{+\bullet}$–$PI^{-\bullet}$–NDI and $Chl^{+\bullet}$–$PI^{-\bullet}$–NDI_2. This initial charge separation is followed by a rapid charge shift from $PI^{-\bullet}$ to NDI and subsequent charge recombination of $Chl^{+\bullet}$–PI–$NDI^{-\bullet}$ and $Chl^{+\bullet}$–PI–(NDI)$NDI^{-\bullet}$ on a 5–30 ns time scale. Charge recombination in the Chl–PI–NDI_2 cyclic tetramer (τ_{CR} = 30 ± 1 ns in toluene) is slower by a factor of 3 relative to the monomeric building blocks (τ_{CR} = 10 ± 1 ns in toluene–1% pyridine). This indicates that the self-assembly of these building blocks into the cyclic tetramers alters their structures in a way that lengthens their charge separation lifetimes, which is an advantageous strategy for artificial photosynthetic systems.

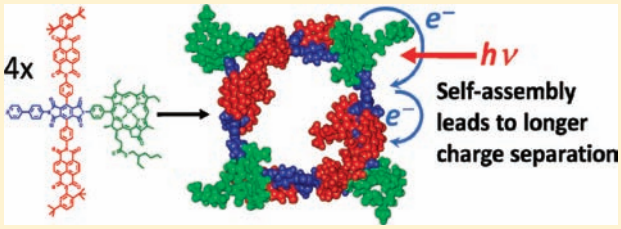

INTRODUCTION

Photophysical studies of biomimetic systems have provided key insights into the mechanisms of energy and electron transfer in natural photosynthesis that are necessary for the development of well-ordered supramolecular systems for artificial photosynthesis. Specifically, understanding how to design molecular building blocks that self-organize into architectures to improve and/or promote light-driven functionality is important for converting solar energy into electricity or fuels.[1] A wide variety of chromophores, including those found in natural photosynthetic proteins, have been utilized as self-assembling molecular building blocks that both collect light energy and carry out charge separation.[1a,2] The tunable electronic and redox properties of natural chlorophyll make it a valuable model for probing electron transfer reactions. Chlorophylls absorb light across a broad range of wavelengths and act as both energy and electron donors and acceptors. Various substituents on the chlorin core give rise to a diverse set of naturally occurring pigments that can be extracted from photosynthetic organisms, isolated, then synthetically modified. For example, most naturally occurring chlorophyll pigments are oxidatively unstable largely because of the *β*-keto ester in their isocyclic E ring. As a consequence, decarboxylation of the *β*-keto ester to give the ketone greatly increases their stability without significantly changing their electronic properties.

Semisynthetic chlorophyll-based systems have been previously shown to undergo efficient photoinduced electron transfer.[3] Recently, we have functionalized zinc methyl 3-ethylpyrochlorophyllide *a* (Chl) at the 20-position to generate a series of donor–acceptor dyads having either a naphthalene-1,8:4,5-bis(dicarboximide) (NDI) or a perylene-3,4:9,10-bis(dicarboximide) (PDI) as the electron acceptor.[4] Upon Chl photoexcitation, ultrafast electron transfer from Chl to NDI or PDI occurs in both polar (τ_{CS} =13–19 ps) and nonpolar (τ_{CS} = 12–25 ps) solvents. In contrast, charge recombination in polar solvents occurs on a picosecond time scale (τ_{CR} = 25–43 ps), while it slows to a nanosecond time scale in nonpolar solvents (τ_{CR} = 1.2–3.3 ns). Although these systems demonstrate nearly unity charge separation quantum yields, their rapid charge recombination in both polar and nonpolar solvents does not allow for applications in artificial photosynthesis, where charge migration and/or chemistry on a slower diffusional time scale are required.

To slow charge recombination, extending the stepwise charge transport array is an advantageous strategy. Following the initial photoinitiated charge separation, natural reaction center proteins use multiple electron transfer steps to increase

Received: December 3, 2011
Published: February 13, 2012

dx.doi.org/10.1021/ja211329k | *J. Am. Chem. Soc.* 2012, 134, 4363–4372

Scheme 1. Donor–Acceptor Triad Structures

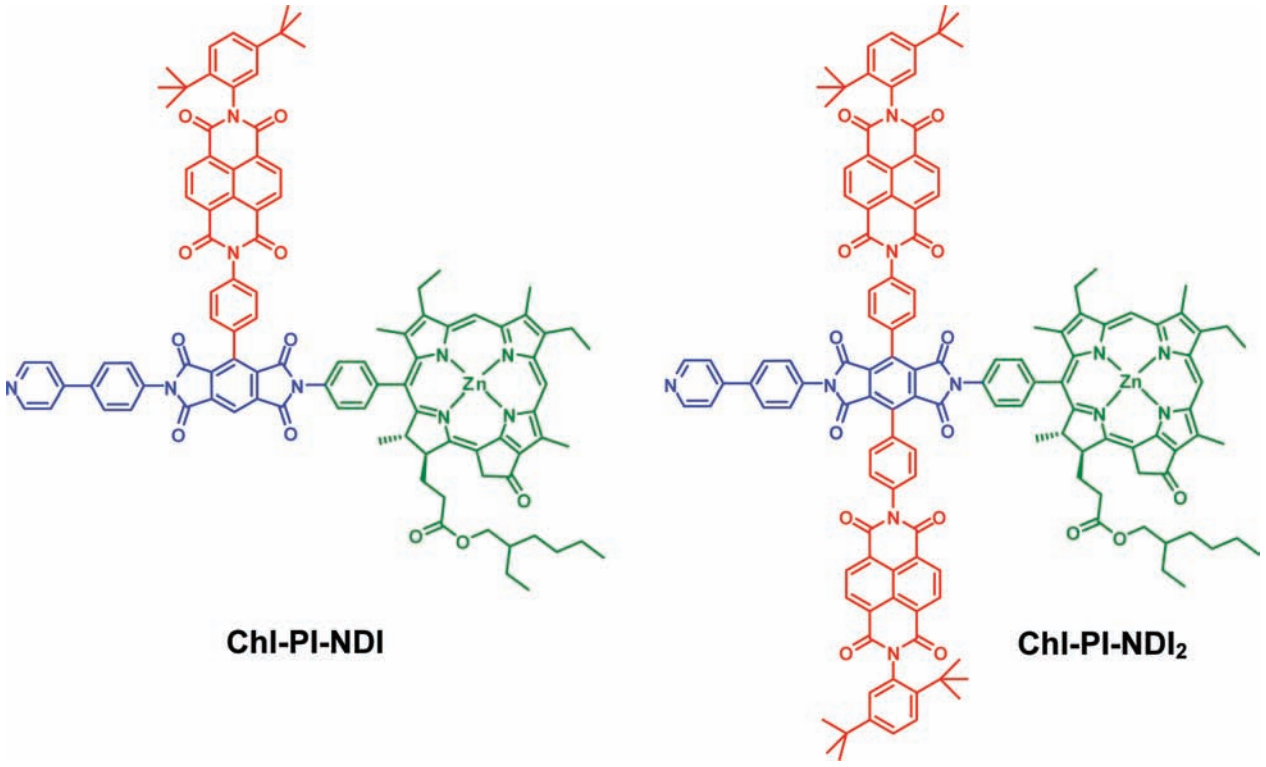

the radical ion pair distances, thereby diminishing the electronic coupling between them and slowing charge recombination.[5] Extension of donor–acceptor dyads to donor–acceptor–acceptor triads has been used to mimic this natural phenomenon.[1d,6] However, this strategy does not always yield optimal systems. For example, a series of molecular dyads and triads have been studied in which zinc methyl 13[1]-desoxopyrochlorophyllide *a* served as the electron donor and was connected through the 3[1]-position to pyromellitimide (PI), NDI, or a serial pair of PI–NDI acceptors.[7] Electron transfer was observed in both dyads and the triad. However, it was shown that the PI one-electron reduction potential is sensitive to the imide substituents. This led to charge separation and recombination lifetimes in the triad that were more rapid relative to the Chl–PI dyad, 2 versus 25 ps and 140 versus 360 ps, respectively, in toluene. Thus, new ways to connect these components that do not perturb the inherent donor and acceptor redox potentials as well as the chromophore excited state energies are necessary to realize long charge separation lifetimes.

The synthesis of such systems often demands considerable effort, so that numerous studies have been directed toward self-assembling large supramolecular structures.[1b,8] Chl's naturally form supramolecular assemblies using metal–ligand coordination as well as hydrogen bonding, $\pi-\pi$ interactions, and hydrophobic effects within the protein environment.[9] For example, Chl's with modifications at the 3-, 8-, and 17-carbon positions have replicated bacteriochlorophyll self-assembly associated with the peripheral antenna complexes of green sulfur bacteria.[10] Additionally, modifications to Chl at the 20-carbon position have also proven useful for producing building blocks leading to discrete self-assembled structures.[11] Specifically, the incorporation of pyridine ligands is a facile strategy for the generation of discrete supramolecular Chl and porphyrin systems, where substitution of a 4-pyridinyl group at the 20-Chl position (or the 5-position of a porphyrin) has led to the assembly of cyclic tetramers (molecular boxes) composed of four self-coordinated Chl (or porphyrin) units, when the monomers are dissolved in nonligating solvents, such as dry toluene.[11a,12] The formation of these supramolecular structures enables new energy transfer pathways to form. However, studies of self-assembled, semisynthetic, Chl-based, electron transfer systems have been limited.[13]

To better determine how self-assembly affects photoinduced charge separation in Chl-based systems, we have synthesized a series of Chl-based donor–acceptor triads (Scheme 1) that self-assemble into cyclic tetramers. Covalent attachment of NDI derivatives to the PI central benzene ring limits perturbation of the PI one-electron reduction potential. This occurs primarily because the large dihedral angle between the attached aromatic group and the PI benzene ring limits transmission of the π substituent effect, and allows for efficient and long-lived charge separation. The incorporation of a pyridine ligand on the donor–acceptor molecular building block further facilitates self-assembly through metal–ligand coordination in toluene. Our results demonstrate that charge separation is stabilized in the self-assembled cyclic arrays relative to that in the corresponding monomers.

EXPERIMENTAL SECTION

Synthesis. The synthesis of the Chl–PI–NDI series is described briefly below and outlined explicitly in the Supporting Information. Chl *a* was extracted from the cyanobacterium *Arthrospira platensis* strain Pacifica obtained from Cyanotech and converted into methyl pyropheophorbide *a*.[14] Selective hydrogenation of the double bond at the 3[1]-position yielded methyl 3-ethyl-pyropheophorbide *a*, which was then brominated at the 20-position.[15] Methyl 20-bromo-3-ethyl-pyropheophorbide *a* underwent a series of reactions to yield zinc 2′-ethylhexyl 3-ethyl-20-(*p*-aminophenyl)-pyropheophorbide *a*.[4] This

dx.doi.org/10.1021/ja211329k | J. Am. Chem. Soc. 2012, 134, 4363–4372

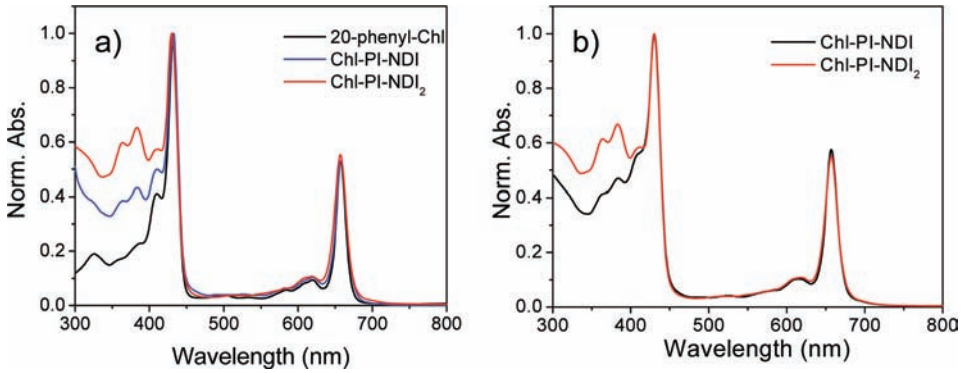

Figure 1. Normalized steady-state absorption spectra in (a) toluene−1% pyridine and (b) toluene.

was further reacted in a series of steps, which included imide condensation reactions with a variety of pyromellitic dianhydride and naphthalene-1,8:4,5-tetracarboxydianhydride derivatives, to yield Chl−PI−NDI, and Chl−PI−NDI_2. The synthetic intermediates and final products were characterized by ^{1}H NMR, MALDI-TOF, MS-ESI, and UV−vis spectroscopy.

Electrochemistry. Electrochemical studies were carried out using a CH Instruments Model 622 electrochemical workstation. The measurements were performed in dichloromethane (DCM) containing 0.1 M tetra-*n*-butylammonium hexafluorophosphate ($TBAPF_6$), and the ferrocene/ferrocenium redox couple (Fc/Fc^+, 0.475 V vs SCE in DCM) was used as an internal reference. A 1.0 mm diameter platinum disk electrode, platinum wire counter electrode, and Ag/AgO_x reference electrode were employed. Sample concentrations were 1 mM. All electrochemical measurements were performed under a dry nitrogen atmosphere. $TBAPF_6$ was purchased from Aldrich and recrystallized twice from ethyl acetate prior to use.

X-ray Scattering. X-ray scattering measurements were performed using the undulator beamline 12-ID at the Advanced Photon Source (APS) at Argonne National Laboratory. The X-ray scattering instrument utilized a double crystal Si(111) monochromator and a two-dimensional mosaic CCD detector.[16] The X-ray wavelength was set at λ = 0.62 Å, and the distance between the sample and detector was adjusted to achieve scattering measured across the 0.007 $Å^{-1} < q <$ 0.027 $Å^{-1}$ region, where $q = (4\pi/\lambda) \sin \theta$, λ is the X-ray scattering wavelength, and 2θ is the scattering angle. A quartz flow cell was used as the sample container. All samples were filtered through 200 nm PTFE filters (Whatman) prior to measurements. The scattering intensity was averaged over 800 measurements, and the solvent scattering was subtracted from the sample spectrum.

Optical Spectroscopy. Steady-state absorption spectroscopy was performed using a Shimadzu 1800 UV/vis spectrophotometer. A single-photon-counting fluorimeter (Photon Technology International) was used for emission experiments. Fluorescence measurements were performed at room temperature in a 1 cm quartz cuvette with excitation/emission geometries at right angles. All solvents were spectroscopic grade and used as is, except for tetrahydrofuran (THF) and toluene, which were further purified by passing them twice through alumina (GlassContour) immediately prior to use.

Femtosecond transient absorption (TA) measurements were made using a Ti:sapphire laser system detailed previously.[17] The instrument response function (IRF) for the pump−probe experiments was 150 fs. Typically 5 s of averaging was used to obtain the transient spectrum at a given delay time. Samples were photoexcited with 416 nm, 110 fs, 1.0 μJ laser pulses focused to a 200 μm spot in a 2 mm path length quartz cuvette. The optical density at the pump wavelength was kept between 0.5 and 0.7. Analysis of the kinetic data was performed at multiple wavelengths using a Levenberg−Marquardt nonlinear least-squares fit to a general sum-of-exponentials function convoluted with a Gaussian instrument response function. In addition, the three-dimensional data set of ΔA versus wavelength and time from 440 to 800 nm and 0−6 ns was analyzed using single value decomposition and global fitting to obtain the decay-associated spectra using Surface Xplorer-Pro.[18]

Samples for nanosecond TA spectroscopy were placed in a 1-cm path length cuvette and excited with 7 ns laser pulses generated using the frequency-tripled output of a Continuum 8000 Nd:YAG laser to pump a Continuum Panther OPO. The laser pulse energy was 1.2 mJ at 416 nm. The excitation pulse was focused to a 5 mm diameter spot and matched to the diameter of the probe pulse generated using a xenon flashlamp (EG&G Electro-Optics FX-200). The signal was detected using a monochromator (HORIBA Triax 180) coupled to a photomultiplier tube (Hamamatsu R926) with high voltage applied only to four dynodes. The total instrument response time was 7 ns and was determined primarily by the laser pulse duration.

Picosecond time-resolved fluorescence (TRF) measurements were made using a streak camera system (Hamamatsu C4780). The light source was a lab-built cavity-dumped Kerr lens mode-locked Ti:sapphire oscillator pumped by a commercial Nd:YVO_4 laser (Spectra-Physics, Millennia V). The center wavelength was 830 nm, and the energy of the 25 fs output pulses was about 30 nJ at a 820 kHz repetition rate. Pump pulses at 415 nm were generated by second harmonic generation in a 200-μm thick LBO (lithium triborate) crystal. A parabolic mirror was used to focus the excitation beam into the sample and the subsequent fluorescence was collected in a back scattering geometry using the same parabolic mirror. Magic angle detection was used to avoid polarization effects. The excitation beam was focused into a 1-cm path length cuvette using a singlet lens. The fluorescence from the sample was collected and focused into a monochromator by a lens pair. The IRF was 20 and 350 ps (fwhm) in 1 and 20 ns time windows, respectively. All data were acquired in single photon counting mode using the Hamamatsu HPD-TA software.

RESULTS AND DISCUSSION

Steady-State Spectroscopy. The ground state absorption spectra of the Chl-based series in toluene−1% pyridine are shown in Figure 1a. The pyridine coordinates to the zinc metal center of the Chl to disrupt self-assembly and yield the spectrum of the monomer. The spectra were normalized at their respective 431 nm B-band (Soret band) maxima. The absorption features observed to the red of the Soret band are also characteristic of the Chl chromophore, where the $Q_y(0,0)$ band maxima for all molecules occur at 658 nm and exhibit only slight extinction coefficient variations between molecules in the series. The sharp absorption features observed at 363 and 383 nm in both Chl−PI−NDI and Chl−PI−NDI_2 result from the NDI acceptor. The extinction coefficient at these wavelengths increases by a factor of 2 upon increasing the number of NDI molecules from Chl−PI−NDI to Chl−PI−NDI_2. For both triads, substitution of the 20-phenyl-Chl macrocycle with PI and NDI results in no discernible 20-phenyl-Chl spectral distortions, which indicates that the electronic coupling between these molecules is weak and that

dx.doi.org/10.1021/ja211329k | J. Am. Chem. Soc. 2012, 134, 4363−4372

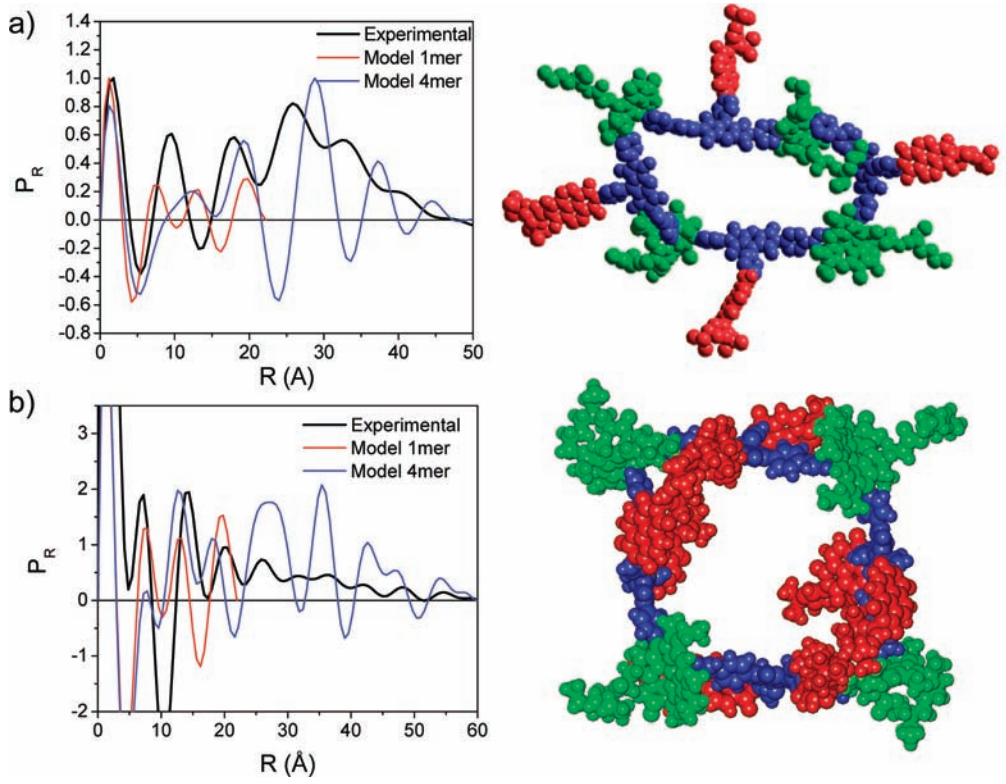

Figure 2. Left: Atomic pair distribution functions (PDFs) obtained from the X-ray scattering data (black) compared with those of the model monomer (red) and model cyclic tetramer (blue) for (a) Chl–PI–NDI and (b) Chl–PI–NDI_2. Right: Structures of cyclic tetramers. The individual donor and acceptors are indicated: Chl (green), PI and spacers (blue), and NDI (red).

these systems are not conjugated supermolecules, but rather as donor–acceptor–acceptor triads. The steady-state absorption spectra of these molecules in dry toluene are shown in Figure 1b. Relative to the absorption spectra of the molecules in toluene–1% pyridine, no significant changes to the spectral features result from the absence of pyridine in solution. The λ_{max} of the Chl Soret band shifts slightly to 429 nm, and the Q_y (0,0) maximum shifts to 657 nm and broadens slightly on its red edge while the NDI peaks do not shift.

When Chl-based systems self-assemble into supramolecular structures, the close proximity of the Chl's usually results in exciton coupling of the Chl transition moments that produces significant spectral shifts of the ground state absorption spectra.[11b,19] These shifts can be used to determine the degree of Chl association and in some favorable cases provide structural information as well. However, in many supramolecular Chl systems, the Chl absorption bands remain unperturbed.[11a,20] The nearly negligible spectral shifts in the Chl–PI–NDI and Chl–PI–NDI_2 ground state absorption spectra in toluene versus toluene–1% pyridine preclude the use of these spectra to study the self-assembly process. Thus, characterizing the self-assembled species requires more advanced techniques.

Characterization of Self-Assembled Structures Using X-ray Scattering. Self-assembly of the Chl–PI–NDI and Chl–PI–NDI_2 building blocks in toluene was probed by small- and wide-angle X-ray scattering (SAXS/WAXS) experiments performed at the Advanced Photon Source at Argonne National Laboratory. The radially averaged scattering intensities for Chl–PI–NDI and Chl–PI–NDI_2 are shown in Supporting Information Figures S1 and S2. In the low-resolution small-angle scattering region, $q < 0.2$ Å^{-1}, the data were fit to the Guinier relationship:

$$I(q) = I(0)\exp(-q^2 {R_g}^2/3) \quad (1)$$

where, $I(0)$ is the forward scattering amplitude and R_g is the radius of gyration of the assembly. A linear Guinier fit over the data range 0.012 Å^{-2} < q^2 < 0.02 Å^{-2} is shown in Figures S1 and S2 (insets), which indicates the formation of discrete molecular aggregates well-approximated by spheres.[21] A least-squares fit to this region reveals that R_g = 17.4 and 15.5 Å for Chl–PI–NDI and Chl–PI–NDI_2, respectively. A comparison of the experimental scattering data with scattering patterns computed for a variety of model structures for Chl–PI–NDI and Chl–PI–NDI_2 aggregates over the range 0.1 Å^{-1} < q < 0.5 Å^{-1} are given in Figures S3 and S4, respectively. The corresponding experimental data for monomeric Chl–PI–NDI and Chl–PI–NDI_2 in toluene–1% pyridine could not be successfully obtained by subtraction of the solvent scattering, presumably as a result of the relatively small size of the monomers.

The linear Guinier fit allows an analysis using atomic pair distribution functions (PDFs) by directly comparing reciprocal-space scattering patterns and real-space molecular models. The experimental PDFs for Chl–PI–NDI and Chl–PI–NDI_2 were obtained using the X-ray scattering fitting program GNOM[22] and model PDFs were generated using the same method from MM+ geometry-optimized models.[23] Figure 2 compares the experimental PDFs of Chl–PI–NDI and Chl–PI–NDI_2 in toluene to those of the corresponding monomer and cyclic tetramer structural models. The number of major atom pair distances and their values determined from the data correlate

dx.doi.org/10.1021/ja211329k | J. Am. Chem. Soc. 2012, 134, 4363–4372

well with the cyclic tetramer models, while the observed discrepancies in PDF peak intensities, that is, "amplitude damping", result from specific solvent interactions with the structures.[24] The Chl−PI−NDI data (Figure 2a) shows significant peak intensities at 17.9, 26.0, and 32.8 Å, with a weaker peak at 39.9 Å, while the corresponding peaks in the static energy-minimized cyclic tetramer model are 19.3, 28.8, and 37.3 Å, with a weaker peak at 44.6 Å. Figure 2a shows that the corresponding monomeric model has no features beyond 20 Å, while alternative oligomeric linear models exhibit a series of features that extend out to 70 Å (Figure S5). Also, forcing the NDI groups to adopt a conformation in which they reside inside the cyclic tetramer does not model the data well (Figure S6). While the cyclic tetramer structure provides the best model for the experimental data, the static model does not capture the dynamic nature of the structure. As distance increases, the linewidths of the experimental PDF features increase as do their deviation from the distances predicted by the static model structure. This most likely reflects both the flexibility of the cyclic structure and the conformational dispersity of Chl, PI, and NDI relative to one another as a result of rotations about their single-bond linkages and the ability of the pyridine to ligate the Chl zinc atom from either of the two nonequivalent faces of the Chl macrocycle.

The corresponding experimental PDF for Chl−PI−NDI_2 shows peaks at 20.1, 26.1, 36.3, 42.1, 48.3, and 54.6 Å, while the model shows peaks at 18.2, 27.1, 35.4, 42.7, 47.1, and 54.2 Å. There is a small peak at 31.8 Å in the experimental data that is not captured in the model; however, the breadth and flat top of the 27.1 Å peak in the model PDF are indicative of two unresolved peaks. The experimental Chl−PI−NDI_2 PDF features are narrower, better resolved, and the predicted distances more closely match those of the cyclic tetramer model relative to what is observed for Chl−PI−NDI. Once again, comparisons of the experimental PDF data with PDFs generated from both monomer and linear oligomer models (Figure S7) show that these models describe the data poorly. The data indicate that the Chl−PI−NDI_2 cyclic tetramer has less conformational dispersity than does Chl−PI−NDI. The additional NDI groups restrict internal rotations within the Chl−PI−NDI_2 cyclic tetramer and essentially provide walls for the box that metal−ligand coordination creates, which is evident in the energy-minimized model shown in Figure 2b.

Charge Transfer Energetics. The one-electron reduction of PI to $PI^{-\bullet}$ was observed at −0.76 V versus SCE, while the one-electron oxidation of 20-phenyl-Chl occurs at 0.63 V versus SCE. PI has been shown to exhibit significant variations in its reduction potential upon substitution at the imide position.[7b,25] However, much smaller potential shifts are observed upon increased substitution of PI on its central benzene core.[26] The one-electron reduction of NDI within Chl−PI−NDI and Chl−PI−NDI_2 occurs at −0.51 V versus SCE; thus, the redox potentials for Chl, PI, and NDI all agree well with previous measurements.[4,27] In a nonpolar solvent (e.g., toluene), the Weller equation can be used to estimate the energy of the initial photogenerated ion pairs ($Chl^{+\bullet}$−$PI^{-\bullet}$−NDI and $Chl^{+\bullet}$−$PI^{-\bullet}$−NDI_2) above the ground state, ΔG_{IP}:[28]

$$\Delta G_{IP} = E_{Ox} - E_{Red} - \frac{e^2}{r_{DA}\varepsilon_S} + e^2\left(\frac{1}{2r_D} + \frac{1}{2r_A}\right) \times \left(\frac{1}{\varepsilon_S} - \frac{1}{\varepsilon_{SP}}\right) \quad (2)$$

where r_{DA} is the donor−acceptor distance, r_D and r_A are the respective ionic radii of the donor and acceptor, ε_S is the static dielectric constant of the nonpolar solvent, ε_{SP} is the static dielectric constant of a high polarity reference, and e is the charge of an electron. A value of r_{DA} = 12.1 Å was determined for the Chl−PI distance using a geometry optimized MM^+ calculation in Hyperchem[23] by estimating the distance from the Chl metal center to the center of the PI benzene ring. The ionic radii for the donor and acceptor were each approximated as $r_{DA}/2$.[29] Using the experimental redox potentials measured in DCM, ΔG_{IP} = 1.80 eV for $Chl^{+\bullet}$−$PI^{-\bullet}$−NDI and $Chl^{+\bullet}$−$PI^{-\bullet}$−NDI_2 in toluene.

The free energies for the initial charge separation (ΔG_{CS1}) and recombination (ΔG_{CR1}) were then determined using eqs 3 and 4, respectively,

$$\Delta G_{CS1} = \Delta G_{IP} - E_S \quad (3)$$

$$\Delta G_{CR1} = -\Delta G_{IP} \quad (4)$$

where the lowest excited singlet state energies (E_S) for Chl were determined by averaging the energies of lowest energy absorption and the highest energy fluorescence maxima of 20-phenyl-Chl, so that E_S = 1.89 eV. The resulting values show that the free energy for the reactions ^{1}*Chl−PI−NDI → $Chl^{+\bullet}$−$PI^{-\bullet}$−NDI and ^{1}*Chl−PI−NDI_2 → $Chl^{+\bullet}$−$PI^{-\bullet}$−NDI_2 are both ΔG_{CS1} = −0.09 eV and ΔG_{CR1} = −1.80 eV, respectively.

For the triad systems, the free energies of the charge shift reactions, $Chl^{+\bullet}$−$PI^{-\bullet}$−NDI → $Chl^{+\bullet}$−PI−$NDI^{-\bullet}$ and $Chl^{+\bullet}$−$PI^{-\bullet}$−NDI → $Chl^{+\bullet}$−PI−(NDI)$NDI^{-\bullet}$ were determined from the difference in redox potentials of the acceptors and the change in Coulomb energy needed to separate the charges farther apart.[6b] Therefore,

$$\Delta G_{IP2} = \Delta G_{IP1} + E_{Red}(PI) - E_{Red}(NDI) - \frac{e^2}{\varepsilon_S}\left(\frac{1}{r_{IP1}} + \frac{1}{r_{IP2}}\right) \quad (5)$$

where ΔG_{IP1} and ΔG_{IP2} are the free energies for the formation of the initial ion pair (IP1) state ($Chl^{+\bullet}$−$PI^{-\bullet}$−NDI and $Chl^{+\bullet}$−$PI^{-\bullet}$−NDI_2) and the final ion pair (IP2) state ($Chl^{+\bullet}$−PI−$NDI^{-\bullet}$ and $Chl^{+\bullet}$−PI−(NDI)$NDI^{-\bullet}$), respectively. As above, the experimental redox potentials for the primary and secondary acceptors were used, and MM+ geometry optimized structures were used to determine the necessary ion pair distances (r_{IP1} = 12.1 Å and r_{IP2} = 14.4 Å). The calculated free energies of the charge shift reactions for both Chl−PI−NDI and Chl−PI−NDI_2 are $\Delta G_{CS2} = \Delta G_{IP2} - \Delta G_{IP1}$ = −0.17 eV, while $\Delta G_{CR2} = -\Delta G_{IP2}$ = −1.63 eV for the distal radical ion pairs.

The free energies for the two charge separation steps offer an interesting contrast to those of the linear dyads/triad studied previously,[7a] which use donors and acceptors that are very similar to those used in the perpendicular triads presented here.

dx.doi.org/10.1021/ja211329k | J. Am. Chem. Soc. 2012, 134, 4363−4372

The major difference between the linear and perpendicular series resides in the connectivity between the redox components. The perpendicular orientation between Chl and the secondary NDI acceptor in the compounds described here results in shorter distance changes between $Chl^{+\bullet}$–$PI^{-\bullet}$–NDI and $Chl^{+\bullet}$–PI–$NDI^{-\bullet}$ relative to those in the linear systems. This decreases the Coulomb energy penalty (last term in eq 5) required to move the opposite charges farther apart in the charge shift reaction, $Chl^{+\bullet}$–$PI^{-\bullet}$–NDI → $Chl^{+\bullet}$–PI–$NDI^{-\bullet}$. Since through-bond electron transfer usually dominates in covalent donor–acceptor molecules, the development of systems with long through-bond pathways and short through-space pathways offers the possibility of minimizing the Coulomb energy penalty without sacrificing the long charge separation lifetimes that are advantageous for artificial photosynthesis.

Charge Transfer Dynamics. Previous photophysical studies on self-assembled Chl-based structures have been directed largely toward understanding Chl–Chl excitation energy transfer (EET) in constructs having multiple identical Chl's.[1a,30] The closest Chl–Chl distances in the self-assembled cyclic tetramers studied here are approximately 19 Å and are thus within a reasonable range to observe Förster-type EET between the Chl's. Using the Förster equation and experimental inputs (see Supporting Information), the predicted EET rate constant between the Chl's in the cyclic tetramers is 2×10^{10} s^{-1} (τ_{EET} = 50 ps). As is seen below, electron transfer from ^{1}*Chl to the PI acceptor is faster in all cases and significant Chl–Chl EET is not observed. The femtosecond transient absorption (fsTA) kinetics are all laser power independent, which indicates that singlet–singlet annihilation does not occur in these systems by EET (Figure S8).[31]

FsTA measurements on the 20-phenyl-Chl electron donor were performed in toluene–1% pyridine using 416 nm, 110 fs excitation pulses (Figure 3). Photoexcitation generates the Chl

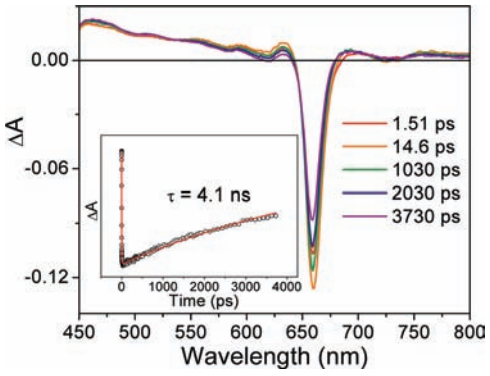

Figure 3. Femtosecond TA spectra of 20-phenyl-Chl in toluene–1% pyridine excited at 416 nm. Inset shows transient kinetics at 667 nm.

S_2 state, which rapidly undergoes internal conversion from S_2 to S_1 within the 150-fs IRF of the experiment.[4,20,31d] The ground state bleach of the $Q_y(0,0)$ band is observed at 658 nm with stimulated emission contributing to the asymmetry of the red edge of the bleach along with a small negative vibronic feature at 725 nm. The broad positive features throughout the spectrum are attributed to ^{1}*Chl absorption, and are punctuated by ΔA due to the ground state bleach. The lifetime of ^{1}*Chl was independently determined using time-resolved fluorescence (TRF) spectroscopy. After photoexcitation with 416 nm, 25 fs pulses, ^{1}*Chl was shown to decay with τ = 4.11 ± 0.03 ns, while analogous experiments in toluene reveal a τ = 3.29 ± 0.02 ns lifetime.

When the Chl-based triads are dissolved in toluene–1% pyridine, the pyridine coordinates to the zinc metal center to disrupt self-assembly. Therefore, it is possible to probe the charge transfer dynamics of the monomeric molecular building blocks in a solvent with nearly the same dielectric constant as the solvent in which the monomers self-assemble into the cyclic tetramers. FsTA spectra for Chl–PI–NDI in toluene–1% pyridine are shown in Figure 4a. Photoexcitation of the Chl Soret band generates ^{1}*Chl, which at early times shows spectral features similar to those of 20-phenyl-Chl (Figure 3). However, as time evolves, a sharp absorption band centered at 726 nm appears, which is characteristic of $PI^{-\bullet}$.[7a] Observation of the spectral changes resulting from the oxidation of ^{1}*Chl to $Chl^{+\bullet}$ is difficult due to their very similar absorption spectra.[4,7a] $Chl^{+\bullet}$ has a weak feature at 820 nm[32] that cannot be observed in these experiments because the cutoff filters needed to eliminate the residual 832 nm laser line block wavelengths near 820 nm from the probe beam.

The disappearance of the spectral features due to $PI^{-\bullet}$ are accompanied by formation of an absorption band at 475 nm, which is characteristic of $NDI^{-\bullet}$,[27] and has been seen in the analogous Chl–NDI dyad.[4,7a] Analysis of the fsTA results using singular value decomposition (SVD) and global fitting[18] yields the decay-associated spectra given in Figure 4b. The resulting time constants, τ_{CS1} and τ_{CS2}, for the two charge separation steps, ^{1}*Chl–PI–NDI → $Chl^{+\bullet}$–$PI^{-\bullet}$–NDI and $Chl^{+\bullet}$–$PI^{-\bullet}$–NDI → $Chl^{+\bullet}$–PI–$NDI^{-\bullet}$, respectively, were determined from the global fitting parameters and the quantum yield of $NDI^{-\bullet}$ as follows. The time constant for the primary charge separation (τ_{CS1}) is obtained directly from the time constant of the decay-associated spectrum given in Figure 4b, green trace, which shows the disappearance of ^{1}*Chl accompanied by the appearance of $PI^{-\bullet}$. Given the 3–4 ns ^{1}*Chl lifetime in 20-phenyl-Chl and its corresponding 8–20 ps lifetimes in the triads, the initial charge separation step (formation of $PI^{-\bullet}$) proceeds with essentially unity quantum yield. To obtain the time constant for the secondary charge shift reaction from $PI^{-\bullet}$ to NDI, the quantum yield of $NDI^{-\bullet}$ formation is needed. As reported earlier,[4] photoexcitation of the corresponding Chl–NDI dyad results in a unity quantum yield of $Chl^{+\bullet}$–$NDI^{-\bullet}$, which produces a transient absorption spectrum for which $|\Delta A_{475nm}/\Delta A_{658nm}|$ = 0.47. The value of the ΔA_{658nm} bleach serves as an internal standard to gauge how much ground state Chl is depleted by the laser pulse. The corresponding ratio observed for $Chl^{+\bullet}$–PI–$NDI^{-\bullet}$ divided by 0.47 gives the $NDI^{-\bullet}$ quantum yield (Table 1). The time constant (τ_{PI}) for the disappearance of $PI^{-\bullet}$ is that of the decay-associated spectrum in Figure 4b, red trace. The rate constant for $PI^{-\bullet}$ disappearance ($k_{PI} = 1/\tau_{PI}$) is assumed to equal $k_{CS2} + k_{CR1}$, where k_{CS2} is the rate constant for charge shift from $PI^{-\bullet}$ to NDI and k_{CR1} is the rate constant for charge recombination of $Chl^{+\bullet}$–$PI^{-\bullet}$–NDI. Thus, $\phi_{NDI} = k_{CS2}/(k_{CS2} + k_{CR1}) = k_{CS2}\tau_{PI}$, or since $\tau_{CS2} = 1/k_{CS2}$, $\tau_{CS2} = \tau_{PI}/\phi_{NDI}$ and thus $\tau_{CR1} = \phi_{NDI}\tau_{CS2}/(1 - \phi_{NDI})$. This analysis is used to obtain τ_{CS1}, τ_{CS2}, τ_{CR1}, and $\phi_{NDI^{-\bullet}}$ for each triad in both toluene–1% pyridine and toluene (Table 1).

FsTA spectroscopy measurements were also performed on Chl–PI–NDI in toluene (Figure 5a), and yield transient spectra similar to those of Chl–PI–NDI in toluene–1% pyridine. The charge separation and recombination time

dx.doi.org/10.1021/ja211329k | J. Am. Chem. Soc. 2012, 134, 4363–4372

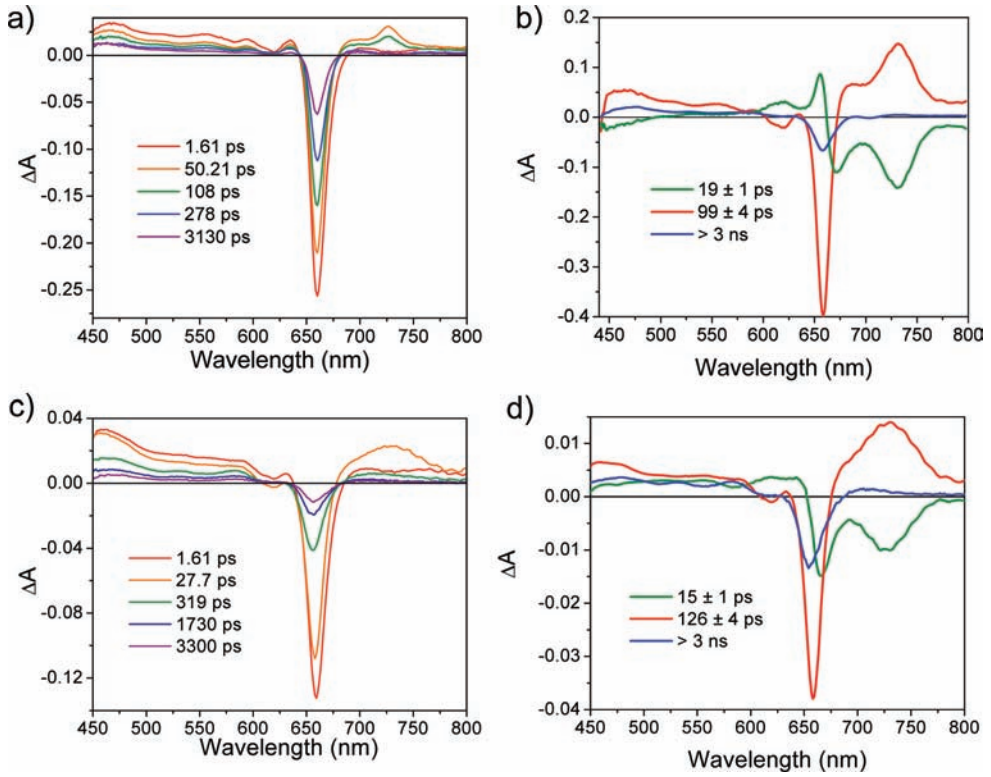

Figure 4. Femtosecond TA spectra and decay-associated spectra of (a and b) Chl–PI–NDI and (c and d) Chl–PI–NDI_2 in toluene–1% pyridine excited at 416 nm.

Table 1. Charge Separation and Recombination Lifetimes and $NDI^{-\bullet}$ Quantum Yields

compound	solvent	τ_{CS1} (ps)	τ_{CS2} (ps)	τ_{CR1} (ps)	τ_{CR2} (ns)	$\phi_{NDI^{-\bullet}}$
Chl–PI–NDI	tol–1% pyr	19 ± 1	148 ± 10	299 ± 10	5–10	0.67 ± 0.05
Chl–PI–NDI	Tol	15 ± 1	518 ± 20	778 ± 30	5–10	0.60 ± 0.05
Chl–PI–NDI_2	tol–1% pyr	15 ± 1	217 ± 10	300 ± 10	10 ± 1	0.58 ± 0.05
Chl–PI–NDI_2	Tol	8 ± 1	827 ± 36	1050 ± 36	30 ± 1	0.56 ± 0.05

constants derived using the analysis described above are summarized in Table 1. Charge recombination of $Chl^{+\bullet}$–PI–$NDI^{-\bullet}$ in both toluene–1% pyridine and toluene occurs with τ_{CR2} = 5–10 ns and is difficult to assess more accurately given the 6 ns limit of the pump–probe delay time of the fsTA apparatus and the 7 ns instrument response function of the nanosecond TA (nsTA) apparatus.

Comparing the Chl–PI–NDI monomer (toluene–1% pyridine) and cyclic tetramer (toluene) data, the initial charge separation (τ_{CS1}) occurs slightly faster in the tetramer. In contrast, the secondary charge shift (τ_{CS2}) slows by about a factor of 3 in the tetramer, yet the quantum yield of $Chl^{+\bullet}$–PI–$NDI^{-\bullet}$ decreases by only about 10%. This is consistent with the fact that the time constant for charge recombination (τ_{CR1}) of $Chl^{+\bullet}$–$PI^{-\bullet}$–NDI also slows in the cyclic tetramer to about the same degree as does τ_{CS2} for the charge shift reaction. Electron transfer theory shows that the rate of charge transfer depends on the free energy of reaction, the total nuclear reorganization energy, and the electronic coupling matrix element for the reaction.[33] The free energies of reaction for CS1 and CS2 do not change appreciably in going from toluene–1% pyridine to toluene because the dielectric constants of these two media are nearly identical and a single pyridine from either the solvent (toluene–1% pyridine) or from the pyridine attached to PI (toluene) is coordinated to the zinc atom of Chl. For the same reasons, in addition to the fact that the distances over which through-bond electron transfer occurs within the Chl–PI–NDI and Chl–PI–NDI_2 building blocks does not change when they form the cyclic tetramers, the total nuclear reorganization energy should not change appreciably. Thus, the observed differences in τ_{CS1}, τ_{CS2}, and τ_{CR1} between the Chl–PI–NDI monomer and the cyclic tetramer most likely result from changes in the electronic coupling matrix elements for charge transfer. While this explanation is consistent with the SAXS/WAXS data, which indicate that cyclic tetramer formation restricts torsional motions about the single bonds linking the donor and acceptors, the scattering data do not provide sufficient structural resolution to identify the relevant dihedral angle changes in the donor–acceptor linkages. Nevertheless, changing torsional conformation distributions in donor–bridge–acceptor molecules has previously been shown to exert significant control over electron transfer rates.[34] It is important to note, however, that restricting the distribution of conformations around the bonds linking the donor and acceptors by assembling supramolecular structures does not necessarily result in a set of conformations that favor charge transfer. Depending on which conformations are important for controlling the electronic coupling matrix elements for charge transfer, self-assembly may result in conformations either favorable or unfavorable for facile charge transfer. Careful

dx.doi.org/10.1021/ja211329k | J. Am. Chem. Soc. 2012, 134, 4363–4372

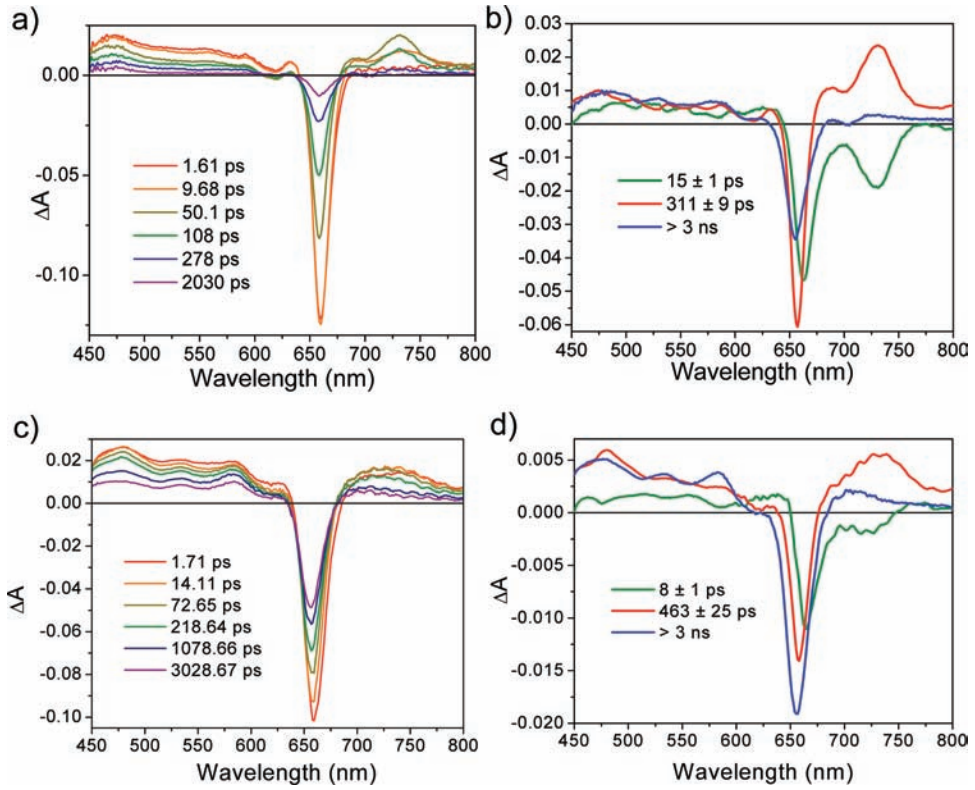

Figure 5. Femtosecond TA spectra and decay-associated spectra of (a and b) Chl−PI−NDI, and (c and d) Chl−PI−NDI_2 in toluene excited at 416 nm.

molecular design is therefore necessary to optimize the supramolecular structure to favor the desired charge transfer rate.

Photoexcitation of Chl−PI−NDI_2 exhibits representative ^{1}*Chl absorption, stimulated emission, and ground state bleach features at 1.6 ps followed within tens of picoseconds by the appearance of the characteristic $PI^{-\bullet}$ absorption band at 726 nm (Figure 4c). The decay-associated spectra show that this $PI^{-\bullet}$ absorption band decays with τ = 126 ± 4 ps (Figure 4d) and is accompanied by the formation of the 480-nm $NDI^{-\bullet}$ band[27] that, in turn, decays on a nanosecond time scale (Figure S9a). NsTA spectroscopy shows that the 480-nm $NDI^{-\bullet}$ absorption decays with biexponential kinetics following photoexcitation of Chl−PI−NDI_2 with 416 nm, 7 ns pulses (Figure S9b). The first decay component (τ_{CR2} = 10 ns) is assigned to $Chl^{+\bullet}$−PI−(NDI)$NDI^{-\bullet}$ charge recombination while the second oxygen-sensitive, residual long-lived component (τ > 300 ns) is assigned to ^{3}*Chl formed by radical pair intersystem crossing[35] of $^1(Chl^{+\bullet}-PI-(NDI)NDI^{-\bullet})$ to $^3(Chl^{+\bullet}-PI-(NDI)NDI^{-\bullet})$ followed by charge recombination.

The corresponding fsTA and nsTA spectra of Chl−PI−NDI_2 in toluene are shown in Figure 5c,d and Figures S9c,d, respectively. The observed trends in τ_{CS1} and τ_{CS2} in comparing the Chl−PI−NDI_2 monomer and cyclic tetramer are similar to those observed for Chl−PI−NDI (Table 1), but are accentuated somewhat, so that τ_{CS1} is shorter by about a factor of 2 and τ_{CS2} is longer by about a factor of 4 in the cyclic tetramer. Once again, there is very little change in the $Chl^{+\bullet}$−PI−(NDI)$NDI^{-\bullet}$ quantum yield between the monomer and the cyclic tetramer, indicating that the charge recombination time constant (τ_{CR1}) of the initial $Chl^{+\bullet}-PI^{-\bullet}-NDI_2$ ion pair also slows commensurately. Given that the SAXS/WAXS data show that the Chl−PI−NDI_2 cyclic tetramer has less structural dispersity than does the corresponding Chl−PI−NDI cyclic tetramer, it is reasonable that greater restriction of torsional angles between the donor and acceptors in the Chl−PI−NDI_2 cyclic tetramer should lead to a larger difference between the monomer and tetramer charge separation rates. This difference is also enhanced in the charge recombination rates (τ_{CR2}) measured by nsTA for the Chl−PI−NDI_2 monomer and cyclic tetramer. The value of τ_{CR2} is a factor of 3 slower in the cyclic tetramer and provides a potentially useful strategy for extending charge separation lifetimes by using self-assembly to control the electronic coupling matrix elements for charge transfer.

■ CONCLUSIONS

Donor−acceptor distances and orientations, their electronic interaction strengths, and free energies of reaction all significantly affect charge transfer rates and efficiencies. The studies described here show how supramolecular assembly can influence photoinduced charge transfer dynamics. Self-assembly of the Chl−PI−NDI and Chl−PI−NDI_2 triads into cyclic tetramers increases their overall charge separation lifetimes and suggests that controlling supramolecular structure can be beneficial for tailoring charge transfer dynamics. The fundamental molecular level understanding gained in such systems provides key design guidance for the fabrication of artificial photosynthetic systems that use self-assembly to generate well-defined supramolecular structures to enhance their photophysical and photochemical functionality.

dx.doi.org/10.1021/ja211329k | J. Am. Chem. Soc. 2012, 134, 4363−4372

■ ASSOCIATED CONTENT

Supporting Information

Experimental details including synthesis, absorption spectra, and additional SAXS/WAXS results and transient absorption spectra and kinetics. This material is available free of charge via the Internet at http://pubs.acs.org.

■ AUTHOR INFORMATION

Corresponding Author

m-wasielewski@northwestern.edu

Notes

The authors declare no competing financial interest.

■ ACKNOWLEDGMENTS

This work was supported by the Chemical Sciences, Geosciences, and Biosciences Division, Office of Basic Energy Sciences, DOE under grant no. DE-FG02-99ER14999. D.T.C. and C.H.K. thank the Initiative for Sustainability and Energy at Northwestern for support.

■ REFERENCES

(1) (a) Wasielewski, M. R. *Acc. Chem. Res.* **2009**, *42*, 1910−1921. (b) Wasielewski, M. R. *J. Org. Chem.* **2006**, *71*, 5051−5066. (c) Magnuson, A.; Anderlund, M.; Johansson, O.; Lindblad, P.; Lomoth, R.; Polivka, T.; Ott, S.; Stensjö, K.; Styring, S.; Sundström, V.; Hammarström, L. *Acc. Chem. Res.* **2009**, *42*, 1899−1909. (d) Gust, D.; Moore, T. A.; Moore, A. L. *Acc. Chem. Res.* **2009**, *42*, 1890−1898. (e) McConnell, I.; Li, G.; Brudvig, G. W. *Chem. Biol.* **2010**, *17*, 434−447. (f) Kalyanasundaram, K.; Graetzel, M. *Curr. Opin. Biotechnol.* **2010**, *21*, 298−310.

(2) (a) Würthner, F. *Chem. Commun.* **2004**, 1564−1579. (b) Chen, Z.; Lohr, A.; Saha-Moeller, C. R.; Wuerthner, F. *Chem. Soc. Rev.* **2009**, *38*, 564−584. (c) Aratani, N.; Kim, D.; Osuka, A. *Acc. Chem. Res.* **2009**, *42*, 1922−1934.

(3) (a) Wasielewski, M. R. In *Chlorophylls*; Scheer, H., Ed.; CRC Press: Boca Raton, FL, 1991; pp 269−286; (b) Regehly, M.; Ermilov, E. A.; Helmreich, M.; Hirsch, A.; Jux, N.; Röder, B. *J. Phys. Chem. B* **2007**, *111*, 998−1006. (c) Shinoda, S.; Tsukube, H.; Nishimura, Y.; Yamazaki, I.; Osuka, A. *Tetrahedron* **1997**, *53*, 13657−13666. (d) Tauber, A. Y.; Helaja, J.; Kilpelainen, I.; Hynninen, P. H. *Acta Chem. Scand.* **1997**, *51*, 88−93.

(4) Kelley, R. F.; Tauber, M. J.; Wasielewski, M. R. *J. Am. Chem. Soc.* **2006**, *128*, 4779−4791.

(5) Blankenship, R. E. *Molecular Mechanisms of Photosynthesis*; Blackwell Science: Oxford, 2002.

(6) (a) Gust, D.; Moore, T. A.; Moore, A. L. In *Mimicking Bacterial Photosynthesis*; Collings, A. F., Critchley, C., Eds.; Wiley-VCH Verlag GmbH & Co. KGaA: Weinheim, Germany, 2006. (b) Greenfield, S. R.; Svec, W. A.; Gosztola, D.; Wasielewski, M. R. *J. Am. Chem. Soc.* **1996**, *118*, 6767−6777. (c) Bullock, J. E.; Carmieli, R.; Mickley, S. M.; Vura-Weis, J.; Wasielewski, M. R. *J. Am. Chem. Soc.* **2009**, *131*, 11919−11929.

(7) (a) Wiederrecht, G. P.; Niemczyk, M. P.; Svec, W. A.; Wasielewski, M. R. *J. Am. Chem. Soc.* **1996**, *118*, 81−88. (b) Wiederrecht, G. P.; Svec, W. A.; Niemczyk, M. P.; Wasielewski, M. R. *J. Phys. Chem.* **1995**, *99*, 8918−8926. (c) Wiederrecht, G. P.; Svec, W. A.; Wasielewski, M. R. In *Ultrafast Phenomena IX*; Barbara, P. F., Knox, W. H., Eds.; Springer-Verlag: Berlin, 1994; Vol. *60*, pp 452−453.

(8) Beletskaya, I.; Tyurin, V. S.; Tsivadze, A. Y.; Guilard, R.; Stern, C. *Chem. Rev.* **2009**, *109*, 1659−1713.

(9) Balaban, T.; Tamiaki, H.; Holzwarth, A. In *Supermolecular Dye Chemistry*; Würthner, F., Ed.; Springer: Berlin/Heidelberg, 2005; Vol. *258*, pp 585−585.

(10) (a) Sasaki, S.-i.; Omoda, M.; Tamiaki, H. *Photochem. Photobiol., A* **2004**, *162*, 307−315. (b) Sasaki, S.-i.; Mizutani, K.; Kunieda, M.; Tamiaki, H. *Tetrahedron Lett.* **2008**, *49*, 4113−4115. (c) Huber, V.; Sengupta, S.; Würthner, F. *Chem.—Eur. J.* **2008**, *14*, 7791−7807.

(11) (a) Kelley, R. F.; Goldsmith, R. H.; Wasielewski, M. R. *J. Am. Chem. Soc.* **2007**, *129*, 6384−6385. (b) Kelley, R. F.; Lee, S. J.; Wilson, T. M.; Nakamura, Y.; Tiede, D. M.; Osuka, A.; Hupp, J. T.; Wasielewski, M. R. *J. Am. Chem. Soc.* **2008**, *130*, 4277−4284.

(12) (a) Jensen, R. A.; Kelley, R. F.; Lee, S. J.; Wasielewski, M. R.; Hupp, J. T.; Tiede, D. M. *Chem. Commun.* **2008**, 1886−1888. (b) Yatskou, M. M.; Koehorst, R. B. M.; Donker, H.; Schaafsma, T. J. *J. Phys. Chem. A* **2001**, *105*, 11425−11431. (c) Kobuke, Y. *Eur. J. Inorg. Chem.* **2006**, *2006*, 2333−2351. (d) Hwang, I.-W.; Kamada, T.; Ahn, T. K.; Ko, D. M.; Nakamura, T.; Tsuda, A.; Osuka, A.; Kim, D. *J. Am. Chem. Soc.* **2004**, *126*, 16187−16187.

(13) (a) Bucks, R. R.; Boxer, S. G. *J. Am. Chem. Soc.* **1982**, *104*, 340−343. (b) Bucks, R. R.; Netzel, T. L.; Fujita, I.; Boxer, S. G. *J. Phys. Chem.* **1982**, *86*, 1947−1955.

(14) Smith, K. M.; Goff, D. A.; Simpson, D. J. *J. Am. Chem. Soc.* **1985**, *107*, 4946−4954.

(15) Kenner, G. W.; McCombie, S. W.; Smith, K. M. *J. Chem Soc., Perkin Trans. 1* **1973**, 2517−2523.

(16) Seifert, S.; Winans, R. E.; Tiede, D. M.; Thiyagarajan, P. *J. Appl. Crystallogr.* **2000**, *33*, 782−784.

(17) Samuel, A. P. S; Co, D. T.; Stern, C. L.; Wasielewski, M. R. *J. Am. Chem. Soc.* **2010**, *132*, 8813−8815.

(18) Surface Xplorer, Ultrafast Systems LLC, Sarasota, FL 34234, USA.

(19) Katz, J. J.; Shipman, L. L.; Cotton, T. M.; Janson, T. R. In *The Porphyrins*; Dolphin, D., Ed.; Academic Press: New York, 1978; Vol. *V*.

(20) Gunderson, V. L.; Mickley Conron, S. M.; Wasielewski, M. R. *Chem. Commun.* **2010**, *46*, 401−403.

(21) Svergun, D. I.; Koch, M. H. J. *Rep. Prog. Phys.* **2003**, *66*, 1735−1782.

(22) Svergun, D. I. *J. Appl. Crystallogr.* **1992**, *25*, 495−503.

(23) Hypercube, Inc., 1115 NW 4th Street, Gainesville, Florida 32601, USA, 1994.

(24) (a) O'Donnell, J. L.; Zuo, X.; Goshe, A. J.; Sarkisov, L.; Snurr, R. Q.; Hupp, J. T.; Tiede, D. M. *J. Am. Chem. Soc.* **2007**, *129*, 1578−1585. (b) Tiede, D. M.; Zhang, R.; Chen, L. X.; Yu, L.; Lindsey, J. S. *J. Am. Chem. Soc.* **2004**, *126*, 14054−14062.

(25) Viehbeck, A.; Goldberg, M. J.; Kovoc, C. A. *J. Electrochem. Soc.* **1990**, *137*, 1460−1466.

(26) Ahrens, M. J.; Sinks, L. E.; Rybtchinski, B.; Liu, W.; Jones, B. A.; Giaimo, J. M.; Gusev, A. V.; Goshe, A. J.; Tiede, D. M.; Wasielewski, M. R. *J. Am. Chem. Soc.* **2004**, *126*, 8284−8294.

(27) Gosztola, D.; Niemczyk, M. P.; Svec, W.; Lukas, A. S.; Wasielewski, M. R. *J. Phys. Chem. A* **2000**, *104*, 6545−6551.

(28) Weller, A. Z. *Phys. Chem* **1982**, *133*, 93−98.

(29) Basilevsky, M. V.; Rostov, I. V.; Newton, M. D. *Chem. Phys.* **1998**, *232*, 189−199.

(30) (a) Miyatake, T.; Tamiaki, H. *Coord. Chem. Rev.* **2010**, *254*, 2593−2602. (b) Balaban, T. S.; Bhise, A. D.; Bringmann, G.; Bürck, J.; Chappaz-Gillot, C.; Eichhöfer, A.; Fenske, D.; Götz, D. C. G.; Knauer, M.; Mizoguchi, T.; Mössinger, D.; Rösner, H.; Roussel, C.; Schraut, M.; Tamiaki, H.; Vanthuyne, N. *J. Am. Chem. Soc.* **2009**, *131*, 14480−14492.

(31) (a) Larsen, J.; Bruggemann, B.; Polivka, T.; Sunderstrom, V.; Akesson, E.; Sly, J.; Crossley, M. J. *J. Phys. Chem. A* **2005**, *109*, 10654−10662. (b) Bruggemann, B.; Herek, J. L.; Sunderstrom, V.; Pullerits, T.; May, V. *J. Phys. Chem. B* **2001**, *105*, 11391−11394. (c) Valkunas, L.; Trinkunas, G.; Liuolia, V.; Grondelle, R. v. *Biophys. J.* **1995**, *69*, 1117−1129. (d) Gunderson, V. L.; Wilson, T. M.; Wasielewski, M. R. *J. Phys. Chem. C* **2009**, *113*, 11936−11942.

(32) Borg, D. C.; Fajer, J.; Felton, R. H.; Dolphin, D. *Proc. Natl. Acad. Sci. U.S.A.* **1970**, *67*, 813−820.

(33) (a) Marcus, R. A. *J. Chem. Phys.* **1956**, *24*, 966−978. (b) Levich, V. G.; Dogonadze, R. R. *Collect. Czech. Chem. Commun.* **1961**, *26*, 193−214. (c) Marcus, R. A. *J. Chem. Phys.* **1965**, *43*, 679−701. (d) Hopfield, J. J. *Proc. Natl. Acad. Sci. U.S.A.* **1974**, *71*, 3640−3644. (e) Jortner, J. *J. Chem. Phys.* **1976**, *64*, 4860−4867.

(34) (a) Davis, W. B.; Ratner, M. A.; Wasielewski, M. R. *J. Am. Chem. Soc.* **2001**, *123*, 7877−7886. (b) Weiss, E. A.; Tauber, M. J.; Kelley, R. F.; Ahrens, M. J.; Ratner, M. A.; Wasielewski, M. R. *J. Am. Chem. Soc.* **2005**, *127*, 11842−11850.
(35) (a) Buckley, C. D.; Hunter, D. A.; Hore, P. J.; McLauchlan, K. A. *Chem. Phys. Lett.* **1987**, *135*, 307−312. (b) Till, U.; Hore, P. J. *Mol. Phys.* **1997**, *90*, 289−296.